



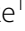






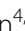



RESEARCH

Open Access



Discrimination between the effects of pulsed electrical stimulation and electrochemically conditioned medium on human osteoblasts

Meike Bielfeldt^{1*} , Kai Budde-Sagert^{2,3} , Nikolai Weis¹ , Maren Buenning¹ , Susanne Staehlke¹ , Julius Zimmermann⁴ , Nils Arbeiter⁴ , Sahba Mobini⁵ , María Ujué González⁵ , Henrike Rebl¹ , Adelinde Uhrmacher^{3,6} , Ursula van Rienen^{4,6}  and Barbara Nebe^{1,6} 

Abstract

Background Electrical stimulation is used for enhanced bone fracture healing. Electrochemical processes occur during the electrical stimulation at the electrodes and influence cellular reactions. Our approach aimed to distinguish between electrochemical and electric field effects on osteoblast-like MG-63 cells. We applied 20 Hz biphasic pulses via platinum electrodes for 2 h. The electrical stimulation of the cell culture medium and subsequent application to cells was compared to directly stimulated cells. The electric field distribution was predicted using a digital twin.

Results Cyclic voltammetry and electrochemical impedance spectroscopy revealed partial electrolysis at the electrodes, which was confirmed by increased concentrations of hydrogen peroxide in the medium. While both direct stimulation and AC-conditioned medium decreased cell adhesion and spreading, only the direct stimulation enhanced the intracellular calcium ions and reactive oxygen species.

Conclusion The electrochemical by-product hydrogen peroxide is not the main contributor to the cellular effects of electrical stimulation. However, undesired effects like decreased adhesion are mediated through electrochemical products in stimulated medium. Detailed characterisation and monitoring of the stimulation set up and electrochemical reactions are necessary to find safe electrical stimulation protocols.

Keywords Electrical stimulation, Alternating current, Osteoblasts, ROS, Calcium ions

Background

The need for long-lasting orthopaedic implants is increasing with the ageing world population. New implant designs strive to increase osseointegration for longer durability. Conductive or piezoelectric biomaterials are under development to enhance bone healing and tissue regeneration [1]. The usage of electrical stimulation (ES) for bone tissue engineering started with the discovery that bone itself has piezoelectric properties [2] and bone formation is seen in areas of negative potentials [3].

Electrical stimulation for bone regeneration can be divided into three modalities. With direct ES, electrodes

*Correspondence:

Meike Bielfeldt
meike.bielfeldt@med.uni-rostock.de

¹ Institute for Cell Biology, Rostock University Medical Center, 18057 Rostock, Germany

² Institute of Communications Engineering, University of Rostock, 18051 Rostock, Germany

³ Institute for Visual and Analytic Computing, University of Rostock, 18051 Rostock, Germany

⁴ Institute of General Electrical Engineering, University of Rostock, 18051 Rostock, Germany

⁵ Instituto de Micro y Nanotecnología, IMN-CNM, CSIC (CEI UAM+CSIC), Isaac Newton 8, E-28760 Tres Cantos, Madrid, Spain

⁶ Interdisciplinary Faculty, University of Rostock, 18051 Rostock, Germany



© The Author(s) 2023. **Open Access** This article is licensed under a Creative Commons Attribution 4.0 International License, which permits use, sharing, adaptation, distribution and reproduction in any medium or format, as long as you give appropriate credit to the original author(s) and the source, provide a link to the Creative Commons licence, and indicate if changes were made. The images or other third party material in this article are included in the article's Creative Commons licence, unless indicated otherwise in a credit line to the material. If material is not included in the article's Creative Commons licence and your intended use is not permitted by statutory regulation or exceeds the permitted use, you will need to obtain permission directly from the copyright holder. To view a copy of this licence, visit <http://creativecommons.org/licenses/by/4.0/>. The Creative Commons Public Domain Dedication waiver (<http://creativecommons.org/publicdomain/zero/1.0/>) applies to the data made available in this article, unless otherwise stated in a credit line to the data.

are implanted directly at the site of damage and ES is delivered via a subcutaneous or external power source. The second method is capacitive coupling, which uses electrodes on the skin on both sides of the fracture with the advantages of not requiring surgical intervention nor charge transfer. The third modality is inductive coupling, where pulsed electromagnetic fields are applied externally [4, 5].

Pre-clinical trials have revealed that the three approaches contributed to enhanced osteogenesis in small animals. However, in large animal models, only direct ES was described to be successful [6]. Clinical studies have observed varying outcomes of enhanced fracture healing but randomised controlled trials are needed to evaluate possible benefits [5, 7]. The discrepancy between these studies comes from different ES modalities as well as the lack of standardised parameters, evaluation criteria and incomplete device and stimulation description or monitoring [5, 6, 8]. Even though various bone growth stimulators are FDA-approved for clinical use [7, 9], after 60 years of research, ES devices for slow-healing or complicated fractures are only occasionally used in the USA and Canada [10]. We focused on direct contact stimulation with the background of finding safe and effective stimulation parameters for electrically active bone implants.

In general, the effects and mechanisms of ES at a molecular and cellular level are only partially understood. For investigating cellular effects of direct contact ES, direct current (DC) stimulation has been applied to mesenchymal stem cells or pre-osteoblasts in vitro. Pre-osteoblasts showed increased cell proliferation, enhanced surface attachment [11, 12] and expression of osteoblastic marker genes [13] upon stimulation. ES also influenced intracellular calcium ion (Ca^{2+}) concentrations, as DC stimulation led to a 45-fold increase in Ca^{2+} levels in osteoblasts [14]. DC stimulation of mesenchymal stem cells prompted the cells towards enhanced osteogenic differentiation and osteogenic gene expression [15, 16]. Also, cells near the cathode exhibited changes in cell orientation, as their cytoskeleton aligned perpendicular to the electrical field [17]. Enhanced differentiation was accompanied by hyperpolarisation of the cell membrane [18].

The physical factor responsible for these effects is still discussed in the field of electrical bone tissue engineering. With direct ES, the cells are exposed to the electric field and the electrochemical products generated at the electrode interface. Direct DC stimulation can generate hydrogen peroxide (H_2O_2) at the cathode and change the pH value [19]. The electrochemical faradic by-products of DC stimulated medium were shown to affect cellular responses and might contribute to osteogenic

differentiation but also cellular damage [20, 21]. In an attempt to reduce electrochemical reactions, experiments have been conducted using alternating current (AC) for direct contact ES. With the alternating current flow, electrochemical reactions can be reversed, as anode and cathode rotate. However, non-reversible faradic reactions can as well occur, when the applied charge exceeds the water window [22]. The AC stimulation parameters such as the waveform, frequency, duty cycle, voltage and current influence the induced charge and differ greatly in the literature [8].

AC stimulation with sinusoidal waveforms increased alkaline phosphatase activity [23], mineralisation and osteogenic gene expression [24]. Proliferation and vascular endothelial growth factor were found to be upregulated when biphasic currents were applied [25]. The application of 20 Hz biphasic, pulsed stimulation enhanced initial attachment and intracellular Ca^{2+} concentration [26]. Recent work suggests that AC stimulation also affects osteoclast viability and gene expression [27]. AC stimulation could therefore be beneficial for bone tissue engineering and facilitate enhanced osseointegration.

However, the effects of electrochemistry on the cells during the AC stimulation have not been studied so far. To differentiate the electrochemical and the electric field effects, we stimulated MG-63 directly or seeded the cells in previously stimulated cell culture medium. Previous studies from our group on physical plasma treatment showed that plasma treated cell culture medium induces the same cellular effects as the plasma treatment itself [28, 29]. We therefore hypothesized that medium, electrically stimulated with alternating currents, also contains electrochemical products such as H_2O_2 , which induce the same effects as the direct ES. As intracellular reactive oxygen species (ROS) and Ca^{2+} play an essential role in cellular reactions to physical stimuli such as ES [30], this study examined these second messengers in connection with biphasic pulsed electrical stimulation. With a complete description and monitoring of our stimulation setup, other researchers can compare and recreate the effects of electrical stimulation.

Materials and methods

Electrical stimulation

For the electrical stimulation (ES), we used a self-build “Mobini chamber” (Fig. 1A). This chamber was first described for DC ES experiments by Mobini et al. [15]. The chamber fits on top of a standard 6-well-plate. L-shaped platinum electrodes are submerged in the culture medium. Three wells are stimulated in series (stimulation), while the other three wells contain electrodes without any applied electrical stimuli (control) (Fig. 1B). The stimulation setup consists of a stimulator

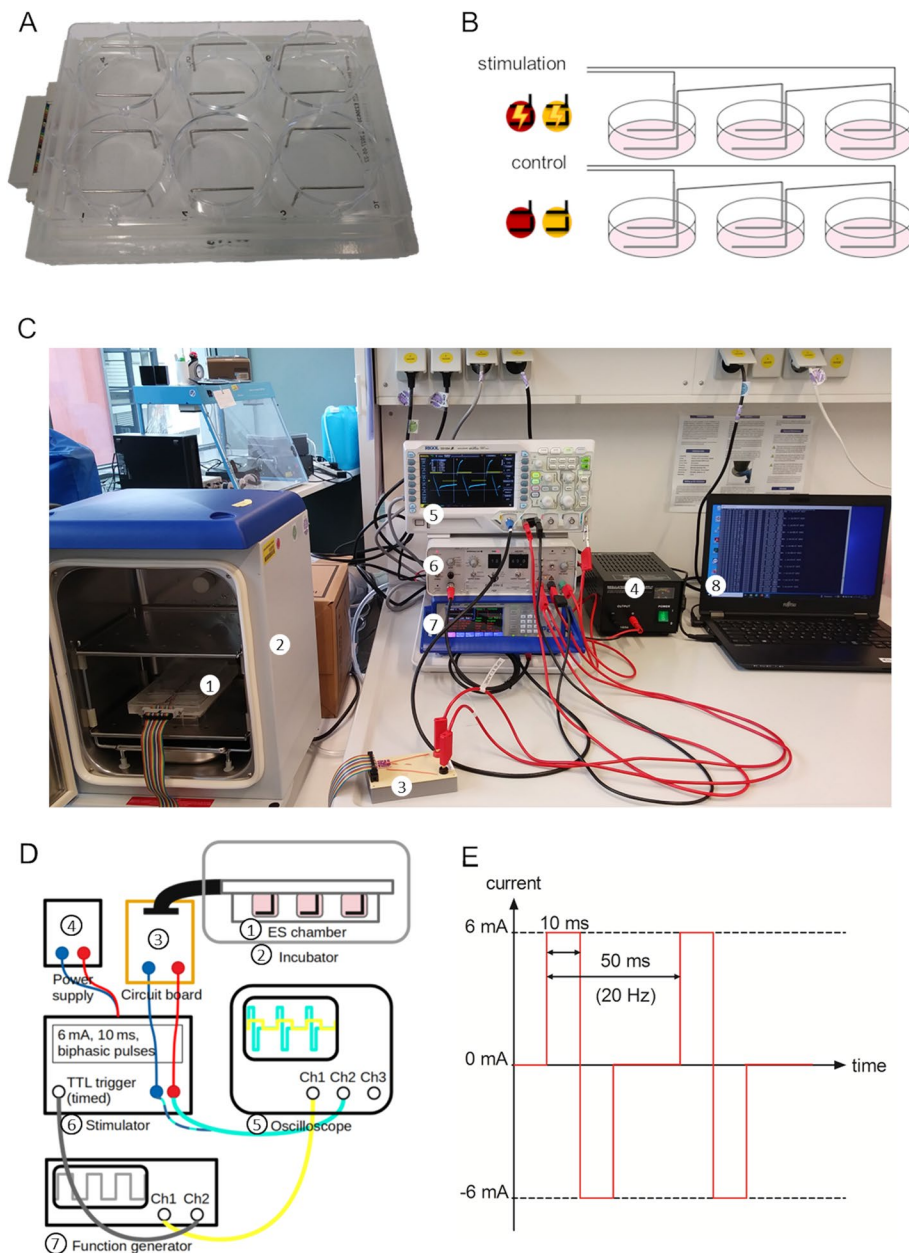


Fig. 1 Electrical stimulation setup. **A** Bottom view of electrode lid (Mobini chamber) in a standard 6-well-plate. **B** Schematic view of Mobini chamber electrode setup and wiring. The symbols with lightning bolt indicate electrical stimulation of cells (red) or cell-free medium (yellow). In the parallel control approach no current was applied (symbols without lightning). **C** View of the stimulation setup with 1) Mobini chamber, 2) incubator, 3) circuit board, 4) power supply, 5) oscilloscope, 6) stimulator, 7) function generator and 8) laptop for data acquisition. **D** Schematic view of the ES setup and wiring. The function generator creates an “on-signal” at 20 Hz frequency. This is used as a trigger for the stimulator to produce the isolated biphasic 6 mA pulses. The resulting applied voltage across the three stimulated wells is measured with an oscilloscope (Ch1 = channel 1, Ch2 = channel 2, TTL trigger = timed transistor-transistor logic trigger). **E** Diagram of the applied current over time

(ISO-STIM-II, npi electronic GmbH, Tamm, Germany) powered by a DC power supply (VOLTcraft FSP-1132, Conrad Electronic SE, Hirschau, Germany) and driven by a function generator (GW Instek MFG-2230M, data-Tec AG, Reutlingen, Germany). The stimulation chamber

was placed in an incubator at 37°C, 5% CO₂. Voltages were monitored using an oscilloscope (digital oscilloscope DS1054, Rigol Technologies Inc., Portland, USA) and the data were recorded on a computer (Fig. 1C,D). For AC stimulation, we applied current-controlled 10 ms

rectangular biphasic pulses with 6 mA and 10 ms pulse width for 2 h at 20 Hz under standard culture conditions directly after cell seeding (Fig. 1E).

Cyclic voltammetry

Electrochemical reactions at the platinum electrodes in cell culture medium were studied via cyclic voltammetry (CV) using a potentiostat (Autolab PGSTAT204, Metrohm AG, Herisau, Switzerland). To perform the CV characterisation, we fabricated a dummy device with two L-shaped Pt electrodes (wire of 0.6 mm diameter, 22 mm distance between electrodes) in a well of a 6-well plate. Therefore, all measurements correspond to a single well. The measurements were performed inside an incubator at standard cell culture conditions, 37 °C and 5% CO₂. The three-electrode configuration was used. The working electrode and counter electrode were assigned arbitrarily to any of the electrodes of the stimulation device, as they are equivalent. An Ag/AgCl electrode (RE-1B, Biologic, Seyssinet-Pariset, France) with 6 mm diameter was used as a reference electrode. 4 ml fresh DMEM (Dulbecco's Modified Eagle Medium) was loaded to the system as electrolyte for each measurement. CV tests were performed within the voltage window (−0.6 V to 0.9 V), where no reactions associated with water hydrolysis have been observed. Moreover, additional CV measurements have been carried out within the extended window (−1.6 V to 2 V) obtained from voltage measurements. In all cases, cycles were performed at a sweep rate of 0.1 V/s and 10 mV step width. Several cycles were run until the system was stable. To determine the CV range, voltages were measured every 100 μs during 100 cycles (5 s) during stimulation. These measurements were carried out in the two electrodes configuration, using the same dummy device employed in the CV characterisation (Additional files Fig. A1).

Electric field simulation and electrochemical impedance spectroscopy

We closely followed the methods described by Zimmermann et al. for the simulation of the applied electric field [31]. Briefly, a calibrated equivalent circuit model comprising the impedance of the electrode-electrolyte interface and the cell culture medium impedance was used to predict the stimulation pulses and the voltage drop across the medium in three wells in series. The calibration data were obtained from electrochemical impedance spectroscopy (EIS) spectra. We conducted the EIS on a single well at different input voltages (10 mV_{rms} to 1 V_{rms}). The impedance spectra were recorded using a Reference 620 potentiostat (GAMRY instruments, Warminster, PA, USA). The conductivity of the cell culture medium DMEM was measured with a handheld conductivity

meter (SevenGo Duo SG23 with probe InLab 751-4 mm, Mettler Toledo, Gießen, Germany) and was measured to be 1.46 Sm^{−1} at 35.5 °C. The probe had been calibrated with conductivity standards in the same range beforehand. The electric field was computed by the finite element method (FEM) using NGSolve 6.2.2102 [32], which is an open-source library for higher-order FEM built on top of the mesh generator NETGEN [33]. The voltage drop across the medium was used to set the boundary conditions in the FEM model.

Cell culture and AC stimulation

Human osteoblast-like cells MG-63 (CRL1427TM, ATCC, Manassas, USA) were cultured in DMEM GlutaMAX (Gibco, Thermo Fisher Scientific) with 10% fetal bovine serum (FBS Superior; Sigma Life Science, Thermo Fisher Scientific) and 1% gentamycin (5 mg/ml, Ratiopharm, Ulm, Germany). Cells were used from passages 5 to 30 [34]. For AC stimulation experiments, 20,000 cells/cm² were seeded on glass coverslips in DMEM without pyruvate (Gibco, Thermo Fisher Scientific) with 10% FBS and 1% gentamycin and electrically stimulated (see above) for 2 h under standard culture conditions at 37 °C and 5% CO₂ (ES cells). DMEM without pyruvate was used, as pyruvate is a scavenger of hydrogen peroxide [35] and we wanted to examine ROS.

To study medium-mediated effects, DMEM without pyruvate was stimulated as described above (ES medium) for 2 h. Cells were seeded in the ES medium shortly after stimulation and incubated for 2 h before further analysis. Cells were cultured up to 24 h after stimulation. To study long lasting effects of ES medium, the stimulated medium was stored at 37 °C, 5% CO₂ for 7 days before cell seeding. For assessment of metabolic activity, cell amount, antioxidant concentration and calcium ion imaging additional experiments were conducted with 1 mM pyruvate (Sigma-Aldrich, Merck KGaA, Darmstadt, Germany) in the medium. As a control, unstimulated medium was supplemented with H₂O₂ (Fluka Analytical, Thermo Fisher Scientific) to a concentration of 10 μM. After ES the electrodes of the “Mobini chamber” were subsequently washed with A. dist., isopropanol (Walter-CMP GmbH & Co. KG, Kiel, Germany) and sterilised in UV light for at least 10 min each.

pH-value and temperature

To assess the impact of ES on DMEM (without pyruvate), the pH value was measured after 2 h ES. Medium containing the electrodes (without ES) served as controls. The pH meter and pH probe with sensor tip (SI series, Sentron Europe BV, Leek, Netherlands) were used outside the incubator. The temperature of the culture medium was measured using an infrared camera

(ThermaCAM™, FLIR Systems AB, Danderyd, Sweden). The camera was placed inside the incubator underneath the culture plate. Measurement points were positioned in the stimulation and control samples near the electrodes. Images of the bottom of the wells were taken every 5 min during treatment.

Scanning electron microscopy and energy dispersive X-ray

Cells and medium were electrically stimulated as described above. Directly after stimulation or 2 h incubation in ES medium, cells were washed in phosphate buffered saline (PBS, Sigma-Aldrich, Merck KGaA, Darmstadt, Germany) and fixed with 2.5% diluted glutaraldehyde solution (Sigma-Aldrich, Merck KGaA). Fixed samples were washed with sodium-phosphate buffer (0.1 M), dehydrated in an ascending series of acetone and critical point dried (Emitech K850, Quorum Technologies LTD, East Sussex, UK). Samples were mounted on Al-SEM-carrier with adhesive conductive carbon tape (PLANO GmbH, Wetzlar, Germany) and coated with carbon (>20 nm, CCU-010HV, safematic GmbH, Zizers, Switzerland) or with gold (20 nm, EM SCD 004, BALTEC, Balzers, Liechtenstein) to reduce accumulation of electrostatic charge. Samples were analysed by a field emission scanning electron microscope (FE-SEM, MERLIN® VP Compact, Carl Zeiss AG, Oberkochen, Germany). Scanning electron microscopy images were taken from the selected regions with accelerating voltage 5 kV, working distance 5.1–5.5 mm. To image the electrodes, the “Mobini chamber” was mounted on a SEM-carrier with adhesive conductive Al-tape (PLANO GmbH). SEM-images were taken from the selected regions. Representative areas or interesting areas of the samples were analyzed for elemental composition with an energy dispersive X-ray detector (XFlash 6/30, Co. Bruker Corporation, USA) by the QUANTAX ESPRIT Microanalysis software (version 2.0). The applied detector and magnification are given in the explanations of the figures.

Cell count and viability

Metabolic activity of adherent cells 24 h after ES treatment was assessed using CellTiter 96® AQueous One Solution Cell Proliferation Assay (MTS; Promega GmbH, Walldorf, Germany). The tetrazolium compound is reduced by NADPH dependent dehydrogenases into a coloured formazan product. The amount of coloured product is therefore dependent on the metabolic activity of viable cells. To compare whether the metabolic activity of the viable cells was changed after ES, the amount of adherent cells was determined with crystal violet staining and used to normalise MTS absorbance.

As described before, 20,000 cells/cm² were AC stimulated for 2 h and incubated at 37°C, 5% CO₂ for 24 h.

Subsequently, non-adherent cells were acquired and cell count and viability were assessed using the NucleoCounter® NC3000™ with the Via1 cassette and Viability and Cell Count Assay (ChemoMetec, Allerød, Denmark). Cells were acquired and stained automatically with DNA binding acridine orange and 4',6-diamidino-2-phenylindole (DAPI). Acridine orange is cell permeable and used to count all cells, while DAPI, which binds to the minor groove of adenine-thymine-rich regions of DNA [36], cannot diffuse across intact cell membranes and is used to stain and count dead cells in this assay. Adherent cells were incubated in MTS assay reagent diluted 1:6 in medium without pyruvate for 2 h. Absorbance was measured at 492 nm with a reference wavelength of 620 nm with a plate reader (anthos Mikrosysteme GmbH, Friesoythe, Germany). Afterwards, the cells were fixated with methanol (Sigma-Aldrich, Merck KGaA) for 10 min and stained with crystal violet (Neisser solution II, Carl Roth GmbH + Co. KG, Karlsruhe, Germany) for 15 min. Cells were washed with distilled water and the staining was extracted using 33% acetic acid (JT Baker, Avantor, Radnor, PA, USA). The absorbance was measured at 620 nm with the plate reader (anthos Mikrosysteme GmbH).

Reactive oxygen species (ROS)

After 2 h ES, H₂O₂ was quantified in DMEM without pyruvate using the fluorimetric hydrogen peroxide assay kit (Sigma-Aldrich, Merck KGaA) according to manufacturer's protocol. H₂O₂ is thereby detected via the reaction with a red peroxidase substrate through horseradish peroxidase and the generation of a fluorescent product. Fluorescence was measured with the fluorescence reader (ex/em: 540/590 nm) (infiniteM200, Tecan Group Ltd., Männedorf, Switzerland) before and after stimulation and H₂O₂ concentration was calculated from standard curve.

Intracellular ROS were detected using the 20,7'-dichlorofluorescein diacetate (DCFDA) assay (Abcam, Cambridge, UK) according to manufacturer's protocol. DCFDA is a membrane-permeable compound that can enter the cells. Inside, cytoplasmic esterases deacetylate the compound into the non-fluorescent DCF. The dye is then oxidised by intracellular ROS, which makes it highly fluorescent. For our experiments, 1 × 10⁶ cells/ml were stained in suspension with 20 μM DCFDA for 30 min in the dark at 37°C. Afterwards, cells were seeded in DMEM without pyruvate and then directly AC stimulated for 2 h. Fluorescence intensity was measured at 485 nm with a fluorescence reader (infiniteM200) before and after stimulation. The fluorescence of non-adherent cells was measured using flow cytometry (FACSCalibur, BD Biosciences, Ann Arbor, MI, USA). To differentiate

ROS signal locations, adherent cells were stained after ES with 5 μ M CellROX green (ROS in nucleus and mitochondria), 5 μ M CellROX orange (ROS in cytoplasm) (Invitrogen GmbH, Darmstadt, Germany) and 9 μ M Hoechst (Life Technologies, Thermo Fisher Scientific) for 30 min at 37°C in the dark. 180 μ M H₂O₂ served as positive control. After incubation the samples were washed with PBS and covered with medium without pyruvate. Images were acquired at random positions in the well and 10 cells per image were analysed using the Zen blue software (LSM 780, 40x/1W Plan-Apochromat water objectiv, Carl Zeiss Microscopy GmbH, Jena, Germany; Software acquisition: Zen black 2.1 V 11.0.0.190; Software analysis: Zen 2.3 blue edition, Carl Zeiss Microscopy).

Antioxidant assay

Intracellular ROS levels are tightly regulated by antioxidants such as ascorbate, glutathione and catalase [37]. In cell culture medium, 1 mM pyruvate is often added, which serves as ROS scavenger. Unspecific antioxidant concentration in cells was measured using the antioxidant assay kit (Cayman chemical, Ann Arbor, MI, USA). In short, the combined antioxidant ability of the sample to suppress the oxidation of ABTS (2,2-azino-bis(3-ethylbenzothiazoline-6-sulfonic acid) by metmyoglobin is compared to a Trolox standard curve.

Stimulated cells were collected in cold assay buffer (Cayman chemical) using a cell scraper. The cells were homogenised by sonication at 35 kHz (Sonorex RK 100, Bandelin electronic, Berlin, Germany) for 5 min. Samples were then centrifuged at 10,000 x g at 4°C for 15 min (Eppendorf centrifuge 5417R, Eppendorf AG, Hamburg, Germany). Subsequently, the supernatant was collected and stored at -80°C. For the assay, samples were thawed and pipetted into a 96-well-plate. ABTS and metmyoglobin were added and the reaction was started by the

addition of H₂O₂. Samples were incubated for 5 min and absorbance was read at 750 nm with a fluorescence reader (infiniteM200, Tecan Group Ltd., Männedorf, Switzerland).

Aquaporins (AQP)

For general AQP expression, cells were cultured in DMEM with 1 mM pyruvate and subsequently processed. MG-63 cells were washed with PBS, trypsinised, and centrifuged (Centrifuge 5810 R, Eppendorf AG) for 5 min at 200 x g. The cells were then fixed with 4% PFA (in PBS, Sigma-Aldrich) at room temperature (RT). Cells were permeabilised with 0.1% Triton X-100 (Sigma-Aldrich) for 10 min at RT. After washing, incubation with 2% FBS (FBS Superior; Sigma Life Science, Thermo Fisher Scientific) in PBS was performed for 1 h to prevent non-specific binding of the primary antibodies. Subsequently, cells were washed and incubated with the primary antibodies at the given dilutions overnight at 4°C (Table 1). The following day, cells were washed and incubated with secondary antibodies for 30 min at RT. Excess antibody was removed and cells were resuspended in 400 μ l PBS and stored at 4°C until analysis. Flow cytometry was performed using the FACSCalibur and Cellquest Pro software (4.0.1). FlowJo software (10.4.2; BD Biosciences) was used for analysis.

Images of AQP 1 were acquired after fixation with ice-cold methanol (99.9%, Sigma Aldrich) for 10 min at 4°C and permeabilised with Triton X-100 for 10 min at RT. Incubation with FBS (2% in PBS) was performed for 1 h, followed by addition of primary AQP 1 antibody (Table 1) and incubating overnight in a wet chamber at 4°C. The samples were washed again with PBS and secondary antibodies were added for 30 min at RT. Fluoroshield mounting medium with DAPI (Fluoroshield™, Sigma-Aldrich) was added to the bottom of the cell container and

Table 1 Antibodies for aquaporin staining

| Antibody | Lot | Supplier | Dilution |
|--|------------|--|---|
| Aquaporin 1 Polyclonal Antibody | 000021263 | Invitrogen GmbH, Darmstadt, Germany | 1:25 in PBS |
| Aquaporin 3 Polyclonal Antibody | B117761 | Invitrogen GmbH, Darmstadt, Germany | 1:25 in PBS |
| Aquaporin 5 Polyclonal Antibody | BJ02243284 | Bioss Antibodies Inc., Woburn, MA, USA | 1:50 in PBS (flow cytometry) 1:100 in PBS (microscopy) |
| Aquaporin 7 Polyclonal Antibody | BA10152932 | Bioss Antibodies Inc., Woburn, MA, USA | 1:50 in PBS (flow cytometry) 1:100 on PBS (microscopy) |
| Aquaporin 8 Polyclonal Antibody | Y03862639B | Invitrogen GmbH, Darmstadt, Germany | 1:50 in PBS (flow cytometry) 1:100 in PBS (microscopy) |
| Aquaporin 9 Polyclonal Antibody | AG10277900 | Bioss Antibodies Inc., Woburn, MA, USA | 1:50 in PBS (flow cytometry) 1:100 in PBS (microscopy) |
| Aquaporin 10 Polyclonal Antibody | R93689 | Invitrogen GmbH, Darmstadt, Germany | 1:25 in PBS |
| Anti-Rabbit IgG Secondary Antibody Alexa Fluor 488 | 1678787 | Life Technologies, Carlsbad, CA, USA | 1:500 in PBS |

Table 2 HEPES buffer composition

| component | | isotonic HEPES | hypotonic HEPES |
|----------------------------------|-------|----------------|-----------------|
| NaCl | [mM] | 137 | 75 |
| HEPES | [mM] | 10 | 10 |
| KCl | [mM] | 5 | 2.75 |
| D-Glucose | [mM] | 5 | 5 |
| Na ₂ HPO ₄ | [mM] | 1 | 1 |
| CaCl ₂ | [mM] | 1 | 1 |
| MgCl ₂ | [mM] | 0.5 | 0.5 |
| Bovine Serum Albumin | [g/L] | 1 | 1 |

covered with a coverslip (Menzel GmbH, Braunschweig, Germany). Samples were then stored at 4°C until analysis with the LSM 780 confocal laser scanning microscope (Carl Zeiss). Images were taken with the Plan-Apochromat 63x oil immersion objective.

Intracellular calcium ion (Ca²⁺) imaging

To evaluate the effects of AC stimulation on MG-63' intracellular Ca²⁺ levels, 20,000 cells/cm² were seeded in 6-well glass bottom plates (Cellvis, Mountain View, CA, USA). Cells were stimulated for 2h directly after seeding as described before. After the stimulation, adherent cells were stained with 5 μM Ca²⁺ sensitive dye Fluo-3 acetoxymethyl ester (AM) (Life Technologies, Thermo Fisher Scientific) for 30 min in HEPES (4-(2-hydroxyethyl)-1-piperazineethanesulfonic acid) buffer (hypotonic and isotonic 1:1, Table 2) [38]. Afterwards, cells were resuspended in isotonic HEPES buffer. For assessment of ES medium on cellular Ca²⁺ levels,

DMEM without pyruvate alone was stimulated for 2h. MG-63 cells were stained with 5 μM Fluo-3/AM in HEPES buffer and seeded in ES medium. Fluorescence images were acquired using a confocal laser scanning microscope (LSM 780, Carl Zeiss Microscopy) with a Plan-Apochromat 63x oil immersion objective (Carl Zeiss Microscopy) and the Zen software (Zen 2.3 SP1 FP3 black, Carl Zeiss Microscopy). Fluorescence intensity was measured using the Zen software (Zen 2.3 blue edition, Carl Zeiss Microscopy). In well-spread cells the Fluo-3 dye and thus the calcium signal is spread over a greater area than in spherical cells. Therefore, bright field images of the LSM were used to determine the cell shape and area. Mean fluorescence intensity (MFI) of Fluo-3 was measured over the whole cell area (Fig. 2).

Statistical analysis

Statistical analysis was performed using Graph Pad Prism 7.02 (GraphPad Software Inc., USA). The graphs show mean values with the standard error of mean (s.e.m). Data was tested for Gaussian distributions using the Shapiro-Wilk normality test. For comparison of multiple samples One-way ANOVA was used and for data, grouped by two or more factors, the two-way ANOVA was applied, both with Bonferroni post-hoc-tests. Where paired data was available for all data points, paired tests were used (RM-ANOVA). Wilcoxon matched-pairs signed rank test was used to test multiple, non-parametric, paired samples. Statistical tests are described in the figure captions. Significance levels are depicted as * $p \leq 0.05$, ** $p \leq 0.01$, *** $p \leq 0.001$ and **** $p \leq 0.0001$.

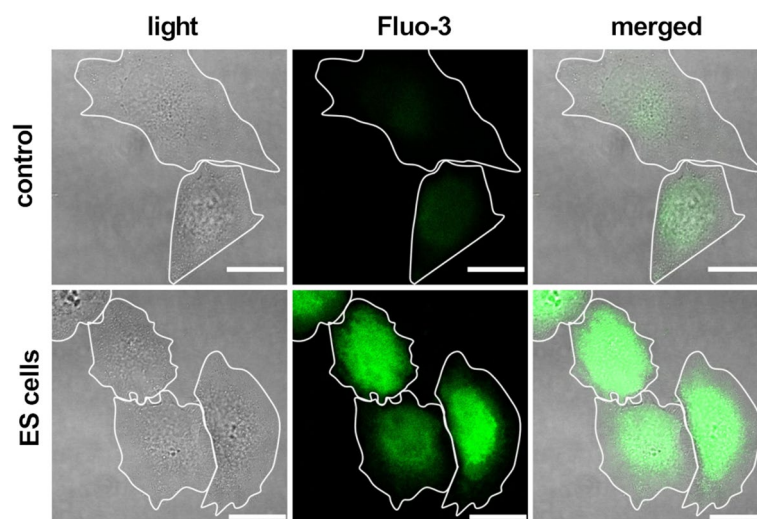


Fig. 2 Image analysis of intracellular Ca²⁺: Mean fluorescence intensity (MFI) of MG-63 osteoblasts stained with Ca²⁺ sensitive dye Fluo-3. Cell shape was determined using light microscopy images from LSM. Then, MFI of Fluo-3 was measured over the whole cell area. (LSM 780, Carl Zeiss, scale bars 20 μm)

Results

Characterisation of the ES chamber and AC stimulation

The application of 6mA current pulses led to the resulting voltage of 14.6 V_{peak to peak} over the three wells in series (Fig. 3A). By dividing the overall voltage by 3, the peak to

peak voltages per well amount to 4.87 V_{peak to peak}. A negative voltage was measured in between the pulses, even though no current was applied. Over the course of the 2h stimulation, this offset decreased. The applied voltage corresponds to the available driving force for electrochemical reactions.

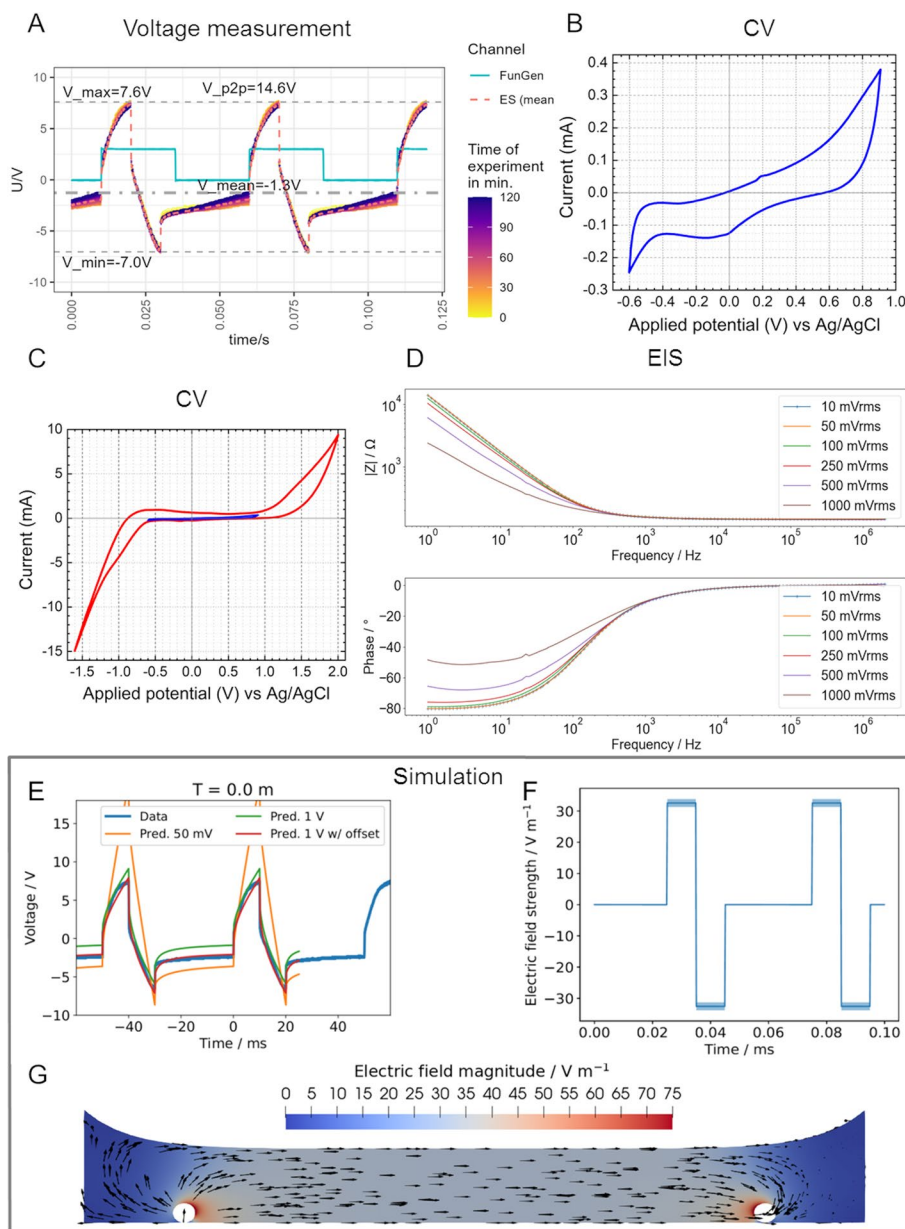


Fig. 3 Characterisation of the electrodes and electric field during electrical stimulation (ES). **A** Voltage measurements over the course of the 2 ES. The colour code indicates the voltage over time. FunGen = 20Hz frequency provided by the function generator. **B** Cyclic voltammetry (CV) was performed with a range from -0.6V to +0.9V. **C** Cyclic voltammogram within the voltage range of -0.6V to +0.9V (blue) compared to the extended range from -1.6V to +2V (red). Note that high currents appear at extended range. **D** Bode plot of electrochemical impedance spectroscopy (EIS). EIS was performed with input voltages from 10 mV_{rms} to 1 V_{rms}. Note that, with input voltages of 0.5 and 1 V_{rms}, the measured impedance ($|Z|$) changes. **E** Prediction of voltage flow from impedance measurements with 50mV (orange), 1V (green), 1V and an arbitrary offset to match the data (red) in comparison to measured voltage flow during experiments (blue). Note that the simulation predicted the waveforms well, when EIS data with 1 V_{rms} input voltage was used. **F** Time-dependent simulated electric field strength in the centre of the well. **G** Simulated electric field distribution in the well. Note that the field is homogeneous except in close proximity to the electrodes

For the electrochemical characterisation of the platinum electrodes, CV was performed. In the normally used range of -0.6 to 1 V, the platinum oxidation and reduction can be seen as an increase in current at 0.2 and -0.1 V respectively (Fig. 3B). We performed the CV also with an extended voltage range in regard to the measured voltages (Fig. 3C). The obtained cyclic voltammogram shows that the voltages attained during ES led to a vast increase in current. We concluded that the voltage window exceeded the water window and electrolysis took place at these points, producing chlorine and hydrogen at the negative potential and oxygen at the positive potential.

Furthermore, we performed EIS measurements for the calibration of the computational model. We found that the impedance measured with a high amplitude of $+1$ V_{rms} led to a different impedance and phase at frequencies under 1 kHz than impedance measured with 10 or 100 V_{rms} (Fig. 3D). This change has an influence on the required voltage. Due to the high input amplitude, non-linear electrochemical effects could be observed. Based on the equivalent circuit model, we predicted the input voltage waveform to see if our model agrees with the experiment. The measured impedance could be successfully described by the equivalent circuit formulated by Zimmermann et al. [31]. However, the initially predicted input voltage from EIS measurements with 50 mV was far off from reality. The predicted waveforms based on EIS measurements with 1 V and the measured waveforms agreed relatively well (Fig. 3E). Additionally, in all stimulations the applied voltages were similar to each other (data available at <https://doi.org/10.5281/zenodo.8262572>).

As the medium is a pure resistor, the voltage drop across the medium should have the same shape as the applied current pulse. This is the reason why we chose current-controlled stimulation. Other than voltage-controlled stimulation, the voltage drop across the medium does in this case only depend on the resistance of the medium. Hence, we estimated the field using the conventional voltage-divider approach described in [31]. The magnitude of the electric field has been estimated to be between 31.3 and 33.8 V/m in the centre of the well (Fig. 3F). The field distribution in the well is homogeneous except for regions in close proximity to the electrodes (Fig. 3G).

Physical changes of cell culture medium

The stimulation resulted in high voltage values up to almost 5 V_{peak to peak} per well. Therefore, as seen in the CV, water breakage is possible during stimulation. After 2 h ES of DMEM culture medium without pyruvate, we found no differences in temperature and pH-value between control and stimulated medium (Table 3). The

temperature increased over the duration of the stimulation, as the samples were placed in an incubator with 37°C as target temperature (Fig. 4A). We further investigated the H₂O₂ concentration before and up to 24 h after ES. The concentration significantly increased after 2 h of AC stimulation up to 12.6 ± 0.85 μM compared to 0.9 ± 0.11 μM in the control samples (electrodes placed in the medium). The concentration of H₂O₂ decreased in both groups over time. After 24 h there was no significant difference between the control (0.18 ± 0.08 μM) and the stimulation (0.83 ± 0.05 μM) (Fig. 4B). When 1 mM pyruvate was added, the H₂O₂ concentration did not increase after ES (Fig. 4C).

Morphology and adhesion

For assessment of the cell morphology, SEM pictures of cells were taken after 2 h ES (Fig. 5A). The control cells on the cover glass were notably spread out. In contrast, the stimulated cells (ES cells) showed a rounder shape with fewer cells spread on the surface. Cells that were able to spread possessed long filopodia and microvilli. As we observed an increased H₂O₂ concentration in stimulated medium, we stimulated medium without cells and immediately seeded the MG-63 cells in ES or control medium. After 2 h the cells were fixated for scanning electron microscopy. ES medium also led to fewer cells spread on the cover glass as seen in ES cell samples. Other than expected, the addition of 10 μM H₂O₂ did not have the same effect on the cells as the ES medium. Cells were able to spread and adhere to the surface (Fig. 5A). The cell area was measured during Ca²⁺ imaging and ES cells were significantly smaller than the controls (Fig. 5B). Cells in ES medium also tended to be smaller than the cells in control medium or 10 μM H₂O₂ control.

Also, 24 h after stimulation, ES samples displayed more non-adherent cells, even though the result was not significant due to high variance (Fig. 5C). Cells incubated in ES medium showed significantly increased numbers of non-adherent cells. At the same time, addition of 10 μM H₂O₂ did not lead to this effect (Fig. 5C). On the other hand, if 1 mM pyruvate was added during the ES, the negative effects on the adhesion were recovered (Fig. 5D). If the stimulated medium without pyruvate was stored for 7 days before cell seeding, also no effect on cell adhesion was detected (Fig. 5E).

Table 3 Culture medium parameter after 2 h ES

| | pH | Temperature [°C] | H ₂ O ₂ [μM] |
|-----------|-----------------|------------------|---|
| control | 7.36 ± 0.02 | 37.97 ± 0.22 | 0.9 ± 0.11 |
| ES medium | 7.35 ± 0.02 | 38.17 ± 0.07 | 12.6 ± 0.85 **** |

Mean \pm s.e.m., $n=3$ individual experiments, paired t -test

**** $p \leq 0.0001$

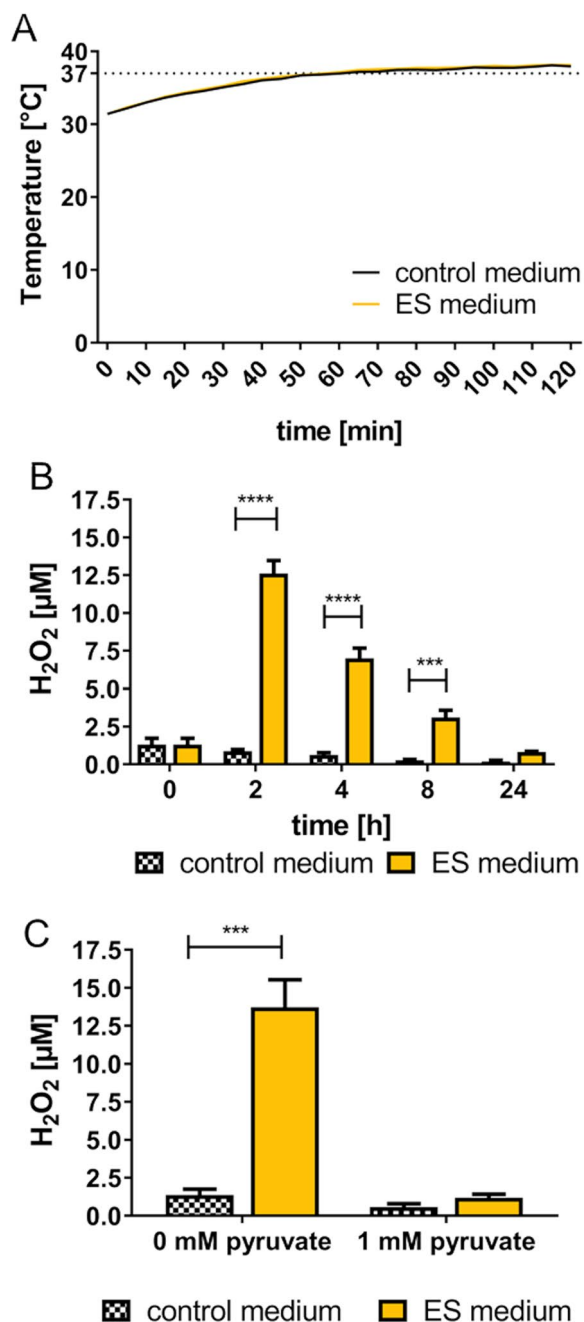


Fig. 4 Changes in the medium induced by 2h AC electrical stimulation (ES). **A** Temperature measurements during ES. Stimulation was performed inside the incubator with a target temperature of 37°C (mean, $n=3$ independent experiments). **B** Significantly higher H₂O₂ concentration in ES medium without pyruvate over the course of 8 h. Note the rapid decline of H₂O₂ up to 24 h (mean \pm s.e.m., $n=2-3$ independent experiments). **C** H₂O₂ concentration after 2h ES in culture medium without and with 1 mM pyruvate added as ROS scavenger (mean \pm s.e.m., $n=3$ independent experiments). B and C: Two-way RM ANOVA with Bonferroni posttests, compared to control

Intracellular ROS production

As the AC stimulation led to increased H₂O₂ concentration in the medium and adversely affected the cell adhesion, we investigated the intracellular ROS response. We investigated directly stimulated, adherent cells using the CellROX staining for ROS in the cytoplasm (CellROX orange) and ROS in the nucleus and mitochondria (CellROX green). Fluorescence microscopy revealed no differences in ROS levels in ES cells compared to the control cells (Fig. 6A,B). The addition of 180 μM H₂O₂ as positive control increased ROS levels significantly, showing the possible maximum in cells' ROS response. Subsequently we also investigated the ROS levels of non-adherent cells after 2h direct and medium mediated ES. For this, cells were stained with the DCFDA assay and measured via flow cytometry (Fig. 6C,D). The ROS level of cells in ES medium did not significantly differ from the control. Directly stimulated ES cells showed an increase of $46 \pm 7.7\%$ compared to the corresponding control. Interestingly, the 10 μM H₂O₂-containing medium significantly increased the cellular ROS levels by $77.8 \pm 19.9\%$.

Antioxidation assay

The concentration of antioxidants in the cells was determined directly after ES. We stimulated the cells with and without 1 mM pyruvate and analysed adherent and non-adherent cells together. Cells stimulated in pyruvate-containing medium showed no difference in antioxidant concentration compared the unstimulated controls. The antioxidant concentration was 0.25 ± 0.02 mM in cells stimulated in medium without pyruvate and therefore significantly lower compared to the control's concentration of 0.29 ± 0.02 mM without pyruvate and $0.30 (\pm 0.03)$ mM with pyruvate (Fig. 6E). The overall decline in antioxidant concentration is in accordance with the increased ROS levels of ES cell samples.

Aquaporins (AQP)

AQPs are water channels of which some are able to transport H₂O₂ through the cell membrane [39]. H₂O₂ is an important by-product of the 2h electrical stimulation system used here (see Fig. 4). Flow cytometry analysis of different AQPs in osteoblast-like MG-63 cells showed higher expression of AQP 1, 5 and 8 compared to AQP 3 and 10 (Fig. 7A). Immunofluorescent staining of AQP 1 showed a signal in the cytoplasm around the nucleus (Fig. 7B).

Calcium ion signalling

As intracellular Ca²⁺ ions are important second messengers, we investigated the Ca²⁺ levels of adherent cells after 2h ES. Interestingly, the position in the well influenced the intracellular calcium signal of the ES cells (Fig. 8A). Images were taken in different regions of the

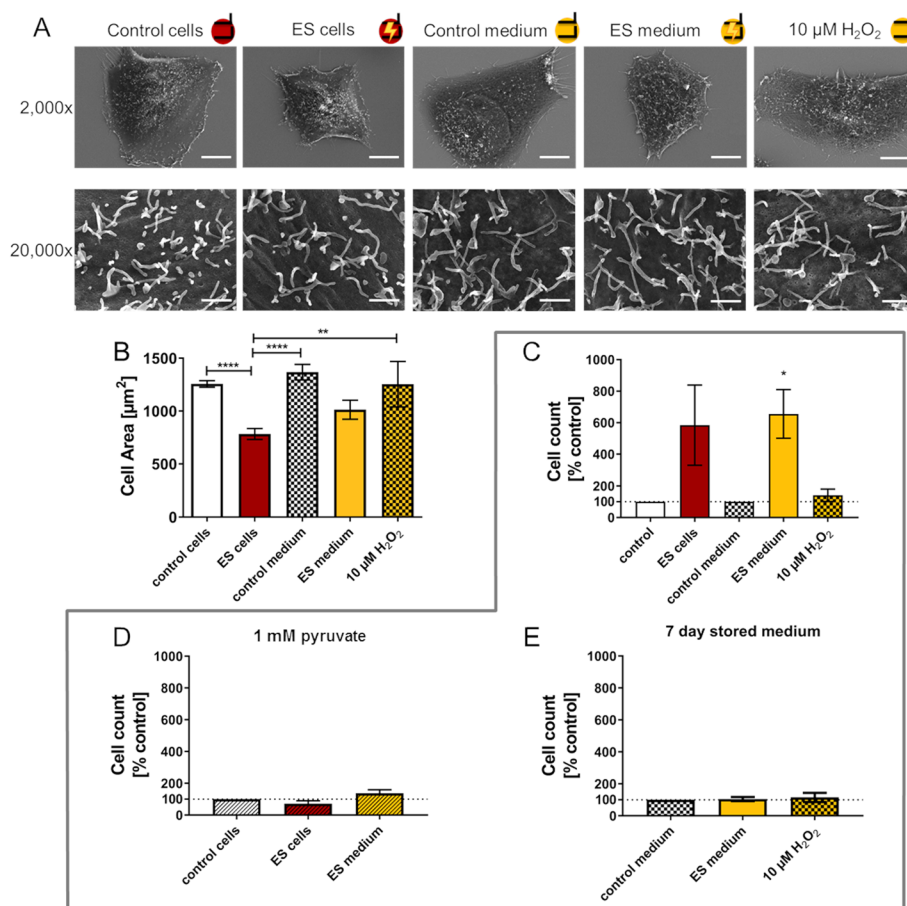


Fig. 5 AC electrical stimulation (ES) influences adhesion of MG-63 cells. **A** Scanning electron microscopy images (SEM) of control cells, AC stimulated cells, cells in stimulated medium and cells in medium containing 10 μM H₂O₂ after 2 h of treatment. Upper row: adherent cells showing smaller cell area after ES (2000x magnification, detector HE-SE 2, scale bar 10 μm). Lower row: microvilli on the cell surface with no obvious changes in length and number (20,000x magnification, detector InLens-Duo, scale bar 1 μm). **B** Cell area of adherent cells after 2 h ES (mean ± s.e.m., n = 4–7 independent experiments, One-way ANOVA with Bonferroni posttest). **C** Quantification of non-adherent cells 24 h after ES (mean ± s.e.m., n = 4 independent experiments, Wilcoxon matched-pairs signed rank test). **D** Quantification of non-adherent cells 24 h after ES with 1 mM pyruvate (mean ± s.e.m., n = 4 independent experiments, Wilcoxon matched-pairs signed rank test). **E** Medium mediated: quantification of non-adherent cells after 24 h in 7 days stored ES medium (mean ± s.e.m., n = 4 independent experiments, Wilcoxon matched-pairs signed rank test). Note that with this setup of 2 h AC both stimulation of cells and medium led to less adherent cells and more non-adherent cells. The addition of 1 mM pyruvate recovered the adhesion during treatment

well: in the middle of the well and at Positions 1 and 2, which were located near the electrodes (Fig. 8B). The Ca²⁺ levels were significantly elevated in ES cells in areas near the electrodes (Fig. 8C). Whereas in the middle of the well cells tended to have increased Ca²⁺ levels but the changes were not significant. This pattern follows the field strength distribution with around 30 V/m in the middle of the well and up to 65 V/m at the electrodes (Fig. 3E). Concerning medium mediated effects, after 2 h in ES medium, cells showed a trend towards increased Ca²⁺ levels compared to cells in control medium (Fig. 8D, E). This increase was not significant or as prominent as in ES cells. Adding 10 μM H₂O₂ also slightly increased

Ca²⁺ levels but did not lead to prominent results as direct stimulation of cells. To investigate the impact of not only H₂O₂ but other ROS during the stimulation, the cells were also directly stimulated in medium supplemented with 1 mM pyruvate. At position 1 near the electrode, the rise in Ca²⁺ concentration through ES was decreased but still significant compared to the control. In the middle of the well no effects of the ES on Ca²⁺ levels were observed. At position 2 near the electrode, ES cells still showed a huge and significantly increased Ca²⁺ signal (Fig. 8F, G).

Taken together, direct stimulation and medium-mediated stimulation are not interchangeable stimulation methods (Table 4). While they both decreased cell

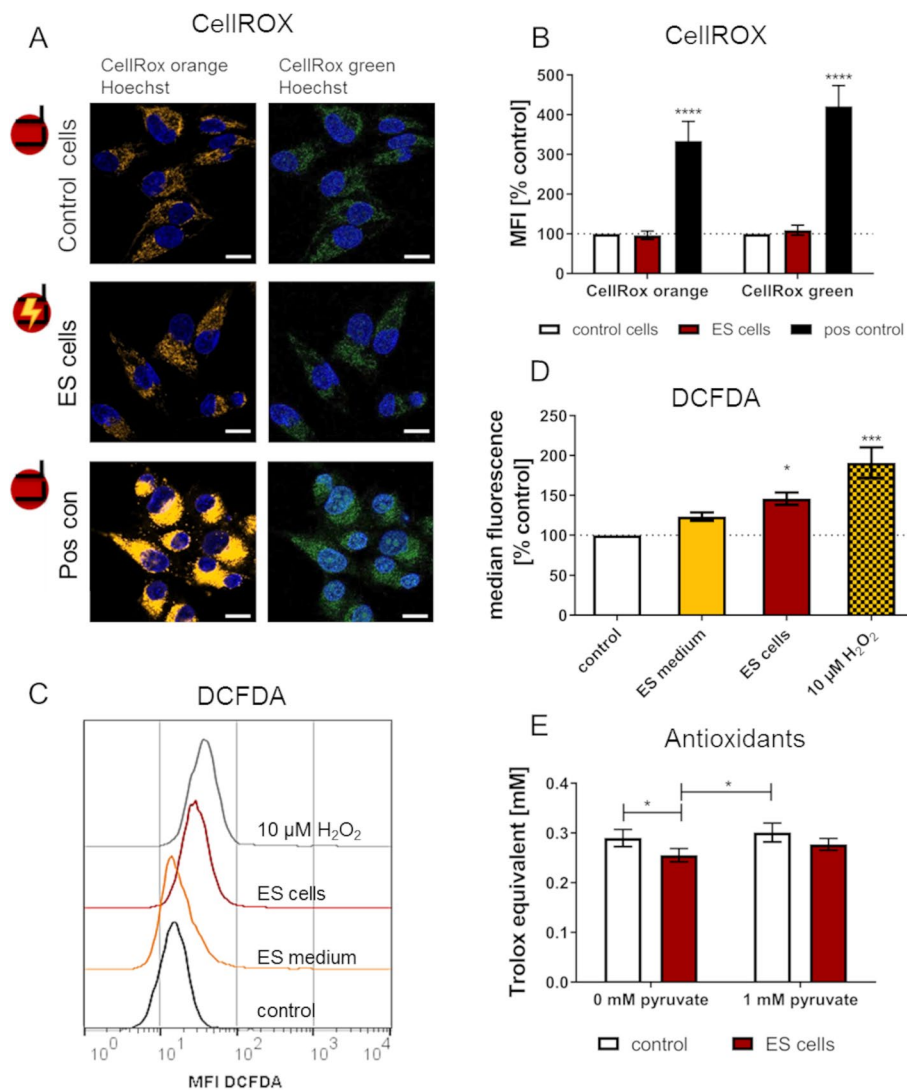


Fig. 6 Electrical stimulation (ES) affects the redox system of MG-63 cells. **A** Fluorescence microscopy of intracellular ROS levels of adherent cells after 2 h ES. Note that ES does not influence intracellular ROS levels (LSM 780, scale bars 20 μm). **B** Mean Fluorescence Intensity (MFI) of ROS in the cytoplasm (CellROX orange) and ROS in the nucleus and mitochondria (CellROX green) (mean ± s.e.m., n = 5 independent experiments á 30–50 cells; Two-way ANOVA with Bonferroni posttests, compared to corresponding control). **C** DCFDA ROS fluorescence of non-adherent cells measured via flow cytometry (representative example of n = 3–4 independent experiments, flow cytometry). **D** DCFDA fluorescence (mean ± s.e.m., n = 3–4 independent experiments; One-way ANOVA with Bonferroni posttests, compared to control). **E** Antioxidant concentration in ES cells stimulated in medium with and without 1 mM pyruvate (mean ± s.e.m., n = 3, Two-way ANOVA with Bonferroni posttests). Note that antioxidant concentration decreased in stimulated cells without pyruvate

adhesion and spreading, the intracellular messengers ROS and Ca²⁺ were increased after direct stimulation but not through medium-mediated treatment. Interestingly, the external addition of 10 μM H₂O₂ had no effect on the adhesion but significantly increased intracellular ROS.

Discussion

Characterisation of the AC stimulation parameters

A digital twin is a model of the stimulation chamber that is continuously updated by measurements. The digital

twin of the stimulation chamber permits to estimate the applied electric field reliably and in accordance with continuously monitored stimulation parameters. An initial guess is formulated based on impedance spectroscopy. Zimmermann et al. already established a digital twin of the “Mobini chamber” [31]. However, the digital twin was only validated for stimulation parameters typical of neural stimulation (in particular, deep brain stimulation). We used the same approach and tested if it could be straightforwardly applied to our parameters.

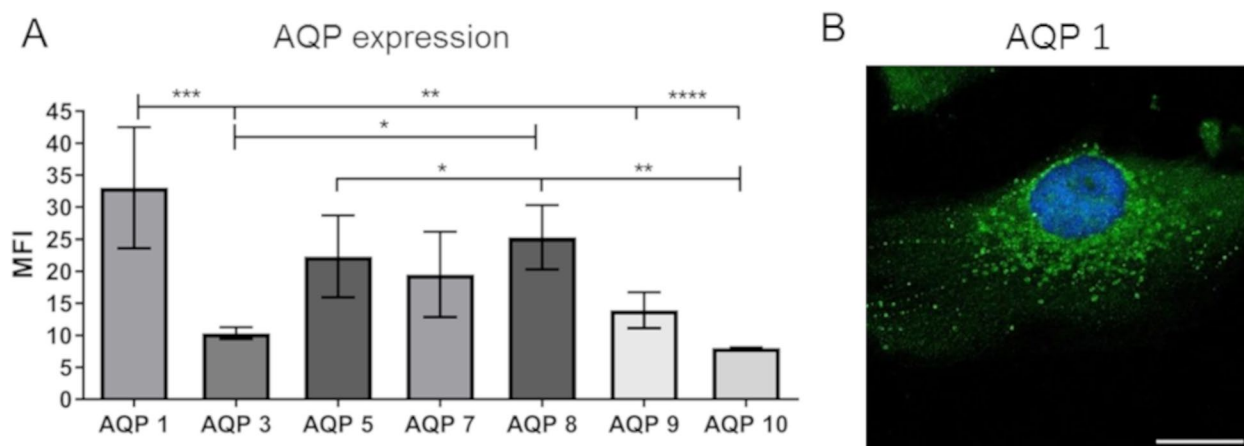


Fig. 7 Aquaporin (AQP) channel expression in MG-63 osteoblasts. **A** Flow cytometry analyses of APQs. Note that AQP 1, as representative for H₂O₂ permeable water channel, is highly expressed (mean ± s.e.m., *n* = 3, One-way ANOVA with Bonferroni posttest). **B** Immunofluorescent staining of AQP 1 (green) and nucleus (blue, DAPI) (LSM 780, scale bar 20 μm)

In contrast to previous results, we found that non-linear electrochemical effects play a significant role when using our stimulation parameters. These effects manifested themselves in the theoretical analysis of the waveforms based on impedance spectroscopy data. Furthermore, both an offset of the applied voltage and a minor waveform change with time could be observed. Merrill et al. described possible electrochemical processes taking place at the platinum electrodes during ES [22]. Aside from the capacitive charging of the electric double layer, reversible and irreversible faradaic reactions with charge transfer can occur, depending on the applied stimuli. Irreversible reactions happen when the counter pulse cannot immediately reverse an electrochemical reaction. Then, reaction products remain in the medium or are released from it. These irreversible reactions lead to a ratcheting of the applied voltage until the same amount of charge is lost during the anodic and cathodic pulse, leading to the observed voltage offset, also being called excess potential or residual voltage [22].

In the field of ES application for bone tissue engineering, many different stimulation systems and parameters are in use [8]. Authors usually report the electric field strength to compare the applied stimulation. However, the methods for obtaining the field strength often remain unnamed and the description of pivotal parameters such as current, voltage, conductivity of the medium and impedance measurements are incomplete [40]. Parameter studies linking specific voltages, frequencies and currents [12, 41, 42] to cellular effects cannot be compared, and the results cannot be applied to other systems. The same problem is seen in pre-clinical trials. A standard set of applied parameters should always be reported [6].

Using the digital twin, we have a reliable electric field estimator at hand. Moreover, we have shown that considerable electrochemical reactions take place that need to be accounted for in interpreting experimental results. We encourage other researchers to follow our example and provide detailed characterisation and monitoring data of their electrical stimulation experiments.

Physical changes of cell culture medium and influence of H₂O₂

After AC stimulation with our parameters using the “Mobini chamber”, the temperature and pH value of the culture medium remained unchanged, while the H₂O₂ concentration was increased to about 12 μM. At high intracellular concentrations, ROS like H₂O₂ react with proteins, lipids, carbohydrates and nucleic acids and can thereby cause functional changes or the destruction of these biomolecules [43]. At moderate concentrations ROS enable redox-dependent biosynthetic processes and are part of signalling pathways [44, 45]. A 10 to 100-fold concentration gradient from extracellular to intracellular H₂O₂ concentration can be assumed, even though higher and lower gradients were described. An extracellular H₂O₂ concentration of 10 μM, as we observed, would therefore result in an intracellular concentration of 0.1 to 1 μM, which is still described to result in beneficial responses [46, 47]. Srirussamee et al. [20] also investigated their cell culture medium for physical changes after DC ES and, similar to our results, found the pH value unchanged and H₂O₂ concentration increased to 5 μM after 2h stimulation [20]. They also treated the cells with the stimulated medium and described cellular effects like decreased metabolic activity. However, it has to be considered that the assay they used shows the amount of metabolically active cells. The measurements

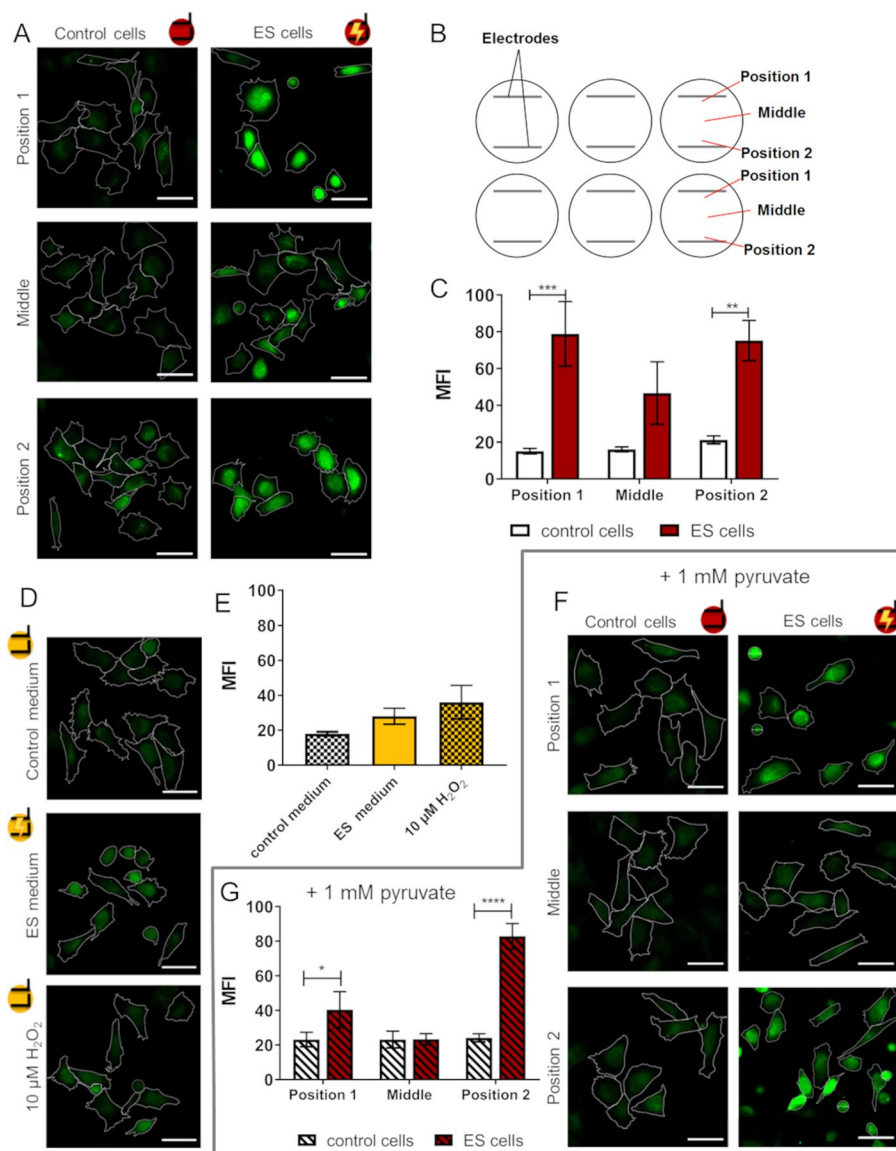


Fig. 8 Intracellular calcium ion (Ca^{2+}) levels are influenced by electrical stimulation (ES). **A** Fluor-3 stained cells directly after 2 h ES at different positions in the well. Note that Ca^{2+} levels are dependent on the position in the well. **B** Schematic view of microscopy positions in the well. Images were taken in the middle and close to the electrode positions. **C** Mean Ca^{2+} fluorescence at the different positions (mean \pm s.e.m., $n=6-7$ independent experiments, \acute{a} 8–30 cells per position, Two-way ANOVA with Bonferroni’s multiple comparison test). **D** Intracellular Ca^{2+} of Fluor-3 stained cells seeded for 2 h in ES medium vs. medium with $10\ \mu\text{M}\ \text{H}_2\text{O}_2$. Note that Ca^{2+} levels are not influenced. **E** Mean Ca^{2+} fluorescence of medium mediated ES (mean \pm s.e.m., $n=4$, RM One-way ANOVA with Bonferroni’s multiple comparison tests, n.s.). **F** Fluor-3 stained cells after direct ES for 2 h in DMEM with pyruvate at different positions of the wells. **G** Mean Ca^{2+} fluorescence of ES cells in pyruvate-containing medium at different positions. Note that Ca^{2+} levels only slightly increase at position 1. (mean \pm s.e.m., $n=6$ independent experiments, \acute{a} 14–38 cells per position, comparison within the positions with RM Two-way ANOVA with Bonferroni’s multiple comparison test). LSM 780, Carl Zeiss, scale bars = $50\ \mu\text{m}$

Table 4 Summary of cellular effects after ES treatment

| | ES cells | ES medium | $10\ \mu\text{M}\ \text{H}_2\text{O}_2$ |
|--------------------------------------|----------|-----------|---|
| Adhesion | ↓ | ↓ | – |
| Intracellular ROS | ↗ | – | ↑ |
| Intracellular Ca^{2+} level | ↑ | – | – |

must be normalised to the number of cells in the sample to describe the metabolic activity. In our experiments, the cell numbers decreased significantly when treated with stimulated medium. When we normalised the metabolic activity to the cell amount, no difference was found between ES and control (Additional files Fig. A2).

Adding 10 μM H_2O_2 to our control medium had neither detrimental nor beneficial effects on cell adhesion. This leads to the conclusion that the H_2O_2 production through ES is not one of the main contributors to the cellular effects. On the other hand, the addition of 1 mM pyruvate to the cell culture medium inhibited the detrimental effects of ES. In another study, Srirussamee et al. [21] also applied 1 h stimulated media to mesenchymal stem cells and found an increase in metabolic activity. When they added 5 mM pyruvate to scavenge ROS, the effect was inhibited [21]. Therefore, H_2O_2 and other ROS might play an important role in bone regeneration. However, radical oxygen or nitrogen species are difficult to detect, as they react with other substances, such as amino acids, ascorbic acid or folic acid [48–50]. Therefore, they are only present for some nano- to microseconds [51].

H_2O_2 cannot diffuse freely through cell membranes but requires channels. Aquaporins (AQP) are a family of transmembrane water channels regulating the transfer of water, gases and small solutes such as urea and glycerol [52]. Some AQPs are also able to transport H_2O_2 across membranes [39]. AQPs 1, 3, 5, 8 and 9 have been described in mammalian cells and human stem cells to be permeable for H_2O_2 [39, 52]. Our results indicate that MG-63 cells express AQP 1, 5, 7 and 8. Therefore, extracellular H_2O_2 may enter the cell, thereby increasing intracellular ROS levels and reducing antioxidant concentration. Surprisingly, although the ES treatment led to increased H_2O_2 concentrations in the medium, ROS levels of cells incubated in ES medium did not significantly increase. Cells incubated in the control medium with 10 μM H_2O_2 showed the largest increase in intracellular ROS levels.

We hypothesise that other factors may interfere in ES samples with the generated H_2O_2 or inhibit the transport through the AQPs. Using the “Mobini chamber”, Srirussamee et al. found enhanced platinum concentrations of 34 $\mu\text{g/L}$ in the culture medium after their ES treatment [21]. On one hand, MG-63 cell culture exposed to platinum showed no growth inhibition or morphological changes [53]. Also, many medical products such as deep brain stimulation electrodes consist of platinum for its good biocompatibility [54]. On the other hand, the dissolution and corrosion of platinum electrodes during stimulation depend on charge density and pulse duration [55]. With our stimulation regime, irreversible reactions at the electrodes are likely to include corrosion of the platinum with chloride ions from the medium ($\text{Pt} + 4\text{Cl}^- \rightarrow [\text{PtCl}_4]^{2-} + 2\text{e}^-$) [22, 55]. However, scanning electron microscopy images and energy dispersive X-ray analysis of the structural and elemental compositions did not show concrete evidence for platinum corrosion (Additional files Fig. A3). On the one hand, the

electrodes, which served as controls, as no current was applied to them, showed a smooth surface with only a few scratches. On the other hand, some electrodes, which were used for the electrical treatment, showed apparent changes of the surface. However, this was only seen in 50% of the stimulated electrodes. As expected, the element analysis showed a high signal intensity for platinum in all samples. Traces of carbon and oxygen were found on some residues, which are likely organic debris. Traces of chloride were found but also sodium chloride crystals. In contrast, in preliminary experiments, platinum could be detected in culture medium after stimulation. Therefore, enhanced platinum concentrations in the medium may also contribute to the cellular effects. Martins et al. showed that metal compounds can inhibit AQP 1 and 3. The gold(III) based complexes were able to inhibit especially AQP 3 in red blood cells, however platinum-based compounds did not show significant effects [56, 57]. Inhibition of AQP 1 by silencing of the expression with shRNA led to decreased extracellular matrix adhesion, proliferation and cell survival in MG-63 cells [58]. Further experiments need to be conducted for a better understanding of possible cellular effects of platinum corrosion products.

Furthermore, we investigated whether stored media still mediates cellular effects after 7 days. For example, medium-mediated effects of physical argon plasma persist even after 7 and 21 days of storage [28, 29]. The authors hypothesised the formation of stable organic peroxides in cell culture medium by plasma-induced ROS chemistry [28]. We found no effects of stored ES medium on cells. Therefore, medium-mediated ES effects were not long-lasting and the DMEM did not preserve the electrochemical characteristics once induced by the electrical stimulation.

Intracellular calcium ion levels

Ca^{2+} is an important intracellular second messenger and changes of intracellular Ca^{2+} concentrations are widely believed to contribute to cellular effects of ES in bone-forming cells [4, 30]. In DC stimulation experiments osteoblast-like cells showed rapidly increased intracellular Ca^{2+} levels upon start of the stimulation [59]. The application of 10 min biphasic stimulation also led to a direct increase of Ca^{2+} [26]. Even though the Ca^{2+} level increase did not persist over 2 days of ES, gene expression of Ca^{2+} signalling pathway-related genes and osteogenesis-related genes were upregulated [60]. Ca^{2+} levels increased up to 45-fold after 20 min of stimulation [14]. In some experiments, the rise of intracellular Ca^{2+} concentration was dependent on the influx of extracellular Ca^{2+} [59]. Other studies reported the increase to be independent of extracellular Ca^{2+} [26] or that the release of

Ca²⁺ from intracellular stores plays a significant role in cytoplasmic Ca²⁺ increase [14].

MG-63 cells showed differences in intracellular Ca²⁺ levels in response to physical factors such as the biomaterial they were cultivated on. Material with moderately positive surface charges showed beneficial effects on cell viability, increased Ca²⁺ levels and enhanced Ca²⁺ mobilisation in MG-63 [61, 62]. Also, mechanical stimulation increased the concentration of intracellular Ca²⁺ via mechano-sensitive ion channels like Piezo1, which is highly important in bone physiology [30, 63]. Enhanced Ca²⁺ levels therefore pointed towards improved cell performances. In contrast, Ca²⁺ also plays a major role in programmed cell death and apoptosis [64]. Disruption of Ca²⁺ homeostasis can also lead to necrotic cell death [65]. ES has been described to induce or inhibit apoptosis depending on the ES parameters. In both cases, increased Ca²⁺ concentrations mediate downstream signalling cascades and the cells' fate [66].

In our experiments, the Ca²⁺ level was found to be increased in regions near the electrodes. Cells in ES medium or H₂O₂ control did not show such a large increase. This effect was therefore not mediated by stable products in the medium and might be a reaction to the electric field. Near the electrodes, the electric field is higher than in the rest of the well and might influence the Ca²⁺ levels. However, when the ROS scavenger pyruvate was added to the culture medium during ES of cells, Ca²⁺ level increase was diminished only at one electrode. At the other electrode, this reduction was not seen. The reason for these position-dependent changes might be the pulsed stimulation with 30 ms stimulation breaks in each cycle. The electrode at position 2 is first the cathode and then the anode during the biphasic stimulation pulse. Cathodic reactions include the reduction of water. Anodic reactions include oxidation of water and corrosion of platinum with chloride ions [22]. While faradic products from the cathodic reaction can be reversed by the anodic pulse, the generated faradic by-products of the anodic phase are not directly reversed. Therefore, locally high concentrations of faradic by-products might also contribute to the increase in intracellular Ca²⁺ at one electrode despite the pyruvate. Intracellular Ca²⁺ and ROS pathways are connected and influence each other. For example, calcium channels in the cell membrane and endoplasmic reticulum are redox-sensitive and modulated by ROS to increase cytosolic Ca²⁺ influx [67, 68].

Switching the electrode connections to change which electrode is cathode first did not change the location of increased Ca²⁺ levels under ES with pyruvate. It seems likely that repeated usage of the "Mobini chamber" has changed the electrodes differently depending on the electrode being anode or cathode first. In the CV experiments, the generated current changed throughout multiple cycles (Additional files

Fig. A4). This effect was described before and was attributed to oxidation of surface atoms, platinum dissolution and re-deposition [69]. The electrochemical potential of each electrode is influenced based on anodic- or cathodic-first pulses [70]. For further biological studies, the platinum electrode surface state should be considered. The different potentials of the electrodes should be prevented by constantly changing the order of the electrodes in the circuit.

Conclusion

We wanted to determine whether electrical stimulation effects on cells are mediated by the electric field or electrochemical products, applied by AC pre-conditioned medium. The direct and indirect, medium-mediated electrical stimulation of MG-63 cells led to decreased adherence of the cells after 2 h alternating current stimulation. When hydrogen peroxide (H₂O₂) was added in the same concentration as measured after electrical stimulation, this effect could not be observed. The cells showed significantly increased intracellular ROS levels when incubated with the 10 μM H₂O₂ control but not with ES medium and only slightly in directly stimulated cells. Neither electrically stimulated medium nor H₂O₂ increased the intracellular calcium levels like direct electrical stimulation of cells did. Therefore, the increased electric field at about 65 V/m at the electrodes might be responsible for the increased intracellular calcium ion concentration. However, as the addition of pyruvate diminished the calcium ion increase, ROS concentration gradients might as well play a part. Taken together, ES led to changes in the culture medium, including the generation of H₂O₂. Nevertheless, the electrical stimulation of the culture medium alone did not induce the same cellular effects as the direct stimulation of cells, indicating the impact of the electric field.

Abbreviations

| | |
|-------------------------------|--|
| AC | alternating current |
| AQP | aquaporin |
| Ca ²⁺ | calcium ions |
| CV | cyclic voltammetry |
| DC | direct current |
| EIS | electrochemical impedance spectroscopy |
| ES | electrical stimulation |
| H ₂ O ₂ | hydrogen peroxide |

Supplementary Information

The online version contains supplementary material available at <https://doi.org/10.1186/s13036-023-00393-1>.

Additional file 1: Fig. A1. Applied voltages measured during stimulation with 6 mA in a single well.

Additional file 2: Fig. A2. Metabolic activity of MG-63 24 h after electrical stimulation (ES) in medium with and without 1 mM pyruvate. A) Electrically stimulated cells. B) Cells incubated in stimulated medium. (Both: mean ± s.e.m., n = 3, Two-way RM ANOVA with Bonferroni posttests).

Additional file 3: Fig. A3. Scanning electron microscopy (SEM) and energy dispersive X-ray (EDX) analysis of the platinum electrodes. A) SEM images of representative electrodes from the "Mobini chamber". Control = no current was applied, ES = electrical stimulation, electrodes were used to deliver 6 mA current pulses. B) EDX measurements for element analysis. C = carbon, Cl = chloride, O = oxygen, Pt = platinum.

Additional file 4: Fig. A4. Impact of electrode cycling on cyclic voltammetry (CV). CV was performed for up to 23 cycles. Note the change in current over the number of cycles.

Acknowledgements

We thank Armin Springer and Karoline Schulz (Electron Microscopy Center, Rostock University Medical Center) concerning SEM analyses. We acknowledge the technical assistance of Petra Seidel (Institute for Cell Biology, Rostock University Medical Center) concerning cell culture. We are thankful to the Institute of Technical Thermodynamics and Michael Reska (FVTR GmbH) for lending us the infrared camera for temperature measurements.

Authors' contributions

M.B. planned and conducted the biological experiments, analysed data and wrote the manuscript. K.B.-S. implemented the stimulation setup and recording, planned experiments and helped with the manuscript. N.W. planned and conducted the biological experiments. M.Bu. planned and conducted the biological experiments. S.S. planned experiments and helped with the manuscript. J.Z. conducted the electric field simulation. N.A. performed the electrochemical impedance spectroscopy. S.M. and M.U.G. planned experiments and performed the cyclic voltammetry measurements. H.R. planned experiments and helped with the manuscript. A.U. planned experiments and helped with the manuscript. U.v.R. acquired the funding and helped with the manuscript. B.N. acquired the funding, planned biological experiments and helped with the manuscript. All authors read and approved the final manuscript.

Funding

Open Access funding enabled and organized by Projekt DEAL. This research was funded by the Deutsche Forschungsgemeinschaft (DFG, German Research Foundation), grant number SFB ELAINE, 1270/1,2–299150580. We also acknowledge the funding from Atracción de Talento Programme, Modalidad-1 Ref. 2019-T1/IND-1335 and the grant PID2021-128611OB-I00 funded by MCIN/AEI/10.13039/501100011033 and by ERDF A way of making Europe.

Availability of data and materials

The datasets supporting the conclusions of this article are available in the zenodo repository <https://doi.org/10.5281/zenodo.8262572>.

Declarations

Ethics approval and consent to participate

Not applicable.

Consent for publication

Not applicable.

Competing interests

The authors declare no competing interests.

Received: 15 September 2023 Accepted: 14 November 2023

Published online: 23 November 2023

References

- Kamel NA. Bio-piezoelectricity: fundamentals and applications in tissue engineering and regenerative medicine. *Biophys Rev.* 2022;14(3):717–33.
- Fukada E, Yasuda I. On the piezoelectric effect of bone. *J Phys Soc Jpn.* 1957;12(10):1158–62.
- Black J. *Electrical stimulation: its role in growth, repair and remodeling of the musculoskeletal system.* Westport, CT: Greenwood Press; 1986.
- Leppik L, Oliveira KMC, Bhavsar MB, Barker JH. Electrical stimulation in bone tissue engineering treatments. *Eur J Trauma Emerg Surg.* 2020;46(2):231–44.
- Griffin M, Bayat A. Electrical stimulation in bone healing: critical analysis by evaluating levels of evidence. *Eplasty.* 2011;11:e34.
- Nicksic PJ, Donnelly DT, Hesse M, Bedi S, Verma N, Seitz AJ, et al. Electronic bone growth stimulators for augmentation of Osteogenesis in vitro and in vivo models: a narrative review of electrical stimulation mechanisms and device specifications. *Front Bioeng Biotechnol.* 2022;10:793945.
- Haglin JM, Jain S, Eltorai AEM, Daniels AH. Bone growth stimulation: a critical analysis review. *JBSJ Rev.* 2017;5(8):e8.
- Pettersen E, Anderson J, Ortiz-Catalan M. Electrical stimulation to promote osseointegration of bone anchoring implants: a topical review. *J Neuroeng Rehabil.* 2022;19(1):31.
- George Shybut BD. OsteoGen™ Surgically Implanted Bone Growth Stimulator - Surgical Technique; 2013. <https://www.zimmerbiomet.eu/content/dam/zb-corporate/en/education-resources/surgical-techniques/specifications/trauma/osteoGen-bone-growth-stimulator/OsteoGenSurgicalTechnique20111.pdf>. Accessed 10 Aug 2023.
- Busse JW, Morton E, Lacchetti C, Guyatt GH, Bhandari M. Current management of tibial shaft fractures: a survey of 450 Canadian orthopedic trauma surgeons. *Acta Orthop.* 2008;79(5):689–94.
- Bodhak S, Bose S, Kinsel WC, Bandyopadhyay A. Investigation of in vitro bone cell adhesion and proliferation on Ti using direct current stimulation. *Mater Sci Eng C Mater Biol Appl.* 2012;32(8):2163–8.
- Pettersen E, Shah FA, Ortiz-Catalan M. Enhancing osteoblast survival through pulsed electrical stimulation and implications for osseointegration. *Sci Rep.* 2021;11(1):22416.
- Martín D, Bocio-Nuñez J, Scagliusi SF, Pérez P, Huertas G, Yúfera A, et al. DC electrical stimulation enhances proliferation and differentiation on N2a and MC3T3 cell lines. *J Biol Eng.* 2022;16(1):27.
- Khatib L, Golan DE, Cho M. Physiologic electrical stimulation provokes intracellular calcium increase mediated by phospholipase C activation in human osteoblasts. *FASEB J.* 2004;18(15):1903–5.
- Mobini S, Leppik L, Barker JH. Direct current electrical stimulation chamber for treating cells in vitro. *Biotechniques.* 2016;60(2):95–8.
- Mobini S, Leppik L, Thottakkattumana Parameswaran V, Barker JH. In vitro effect of direct current electrical stimulation on rat mesenchymal stem cells. *PeerJ.* 2017;5:e2821.
- Mobini S, Talts Ü-L, Xue R, Cassidy NJ, Cartmell SH. Electrical stimulation changes human mesenchymal stem cells orientation and cytoskeleton organization. *J Biomater Tissue Eng.* 2017;7(9):829–33.
- Bhavsar MB, Cato G, Hauschild A, Leppik L, Costa Oliveira KM, Eischen-Loges MJ, et al. Membrane potential (Vm) measurements during mesenchymal stem cell (MSC) proliferation and osteogenic differentiation. *PeerJ.* 2019;7:e6341.
- Bodamyali T, Kanczler JM, Simon B, Blake DR, Stevens CR. Effect of faradic products on direct current-stimulated calvarial organ culture calcium levels. *Biochem Biophys Res Commun.* 1999;264(3):657–61.
- Srirussamee K, Mobini S, Cassidy NJ, Cartmell SH. Direct electrical stimulation enhances osteogenesis by inducing Bmp2 and Spp1 expressions from macrophages and preosteoblasts. *Biotechnol Bioeng.* 2019;116(12):3421–32.
- Srirussamee K, Xue R, Mobini S, Cassidy NJ, Cartmell SH. Changes in the extracellular microenvironment and osteogenic responses of mesenchymal stem/stromal cells induced by in vitro direct electrical stimulation. *J Tissue Eng.* 2021;12:2041731420974147.
- Merrill DR, Bikson M, Jefferys JGR. Electrical stimulation of excitable tissue: design of efficacious and safe protocols. *J Neurosci Methods.* 2005;141(2):171–98.
- Sahm F, Ziebart J, Jonitz-Heincke A, Hansmann D, Dauben T, Bader R. Alternating electric fields modify the function of human osteoblasts growing on and in the surroundings of titanium electrodes. *Int J Mol Sci.* 2020;21(18)
- Sahm F, Freiin Grote V, Zimmermann J, Haack F, Uhrmacher AM, van Rienen U, et al. Long-term stimulation with alternating electric fields modulates the differentiation and mineralization of human pre-osteoblasts. *Front Physiol.* 2022;13:965181.
- Kim IS, Song JK, Zhang YL, Lee TH, Cho TH, Song YM, et al. Biphasic electric current stimulates proliferation and induces VEGF production in osteoblasts. *Biochim Biophys Acta.* 2006;1763(9):907–16.

26. Staehle S, Bielfeldt M, Zimmermann J, Gruening M, Barke I, Freitag T, et al. Pulsed electrical stimulation affects osteoblast adhesion and calcium ion signaling. *Cells*. 2022;11(17)
27. Kreller T, Zimmermann J, van Rienen U, Boccaccini AR, Jonitz-Heincke A, Detsch R. Alternating electric field stimulation: phenotype analysis and osteoclast activity of differentiated RAW 264.7 macrophages on hydroxyapatite-coated Ti6Al4V surfaces and their crosstalk with MC3T3-E1 pre-osteoblasts. *Biomater Adv*. 2023;146:213285.
28. Hoentsch M, Bussiahn R, Rebl H, Bergemann C, Eggert M, Frank M, et al. Persistent effectivity of gas plasma-treated, long time-stored liquid on epithelial cell adhesion capacity and membrane morphology. *PLoS One*. 2014;9(8):e104559.
29. Bergemann C, Gerling T, Hoppe C, Karmazyna M, Höntsch M, Eggert M, et al. Physicochemical analysis of argon plasma-treated cell culture medium. In: Mieno T, editor. *Plasma science and technology - Progress in physical states and chemical reactions*. InTech; 2016.
30. Bielfeldt M, Rebl H, Peters K, Sridharan K, Staehle S, Nebe JB. Sensing of physical factors by cells: electric field, mechanical forces, physical plasma and light—importance for tissue regeneration. *Biomed Mater Devices*. 2022;
31. Zimmermann J, Budde K, Arbeiter N, Molina F, Storch A, Uhrmacher AM, et al. Using a digital twin of an electrical stimulation device to monitor and control the electrical stimulation of cells in vitro. *Front Bioeng Biotechnol*. 2021;9:765516.
32. Schöberl J. C++ 11 implementation of finite elements in NGSolve; 2014. <https://citeseerx.ist.psu.edu/viewdoc/download?repid=rep1&type=pdf&doi=10.1.1.725.9040>. Accessed 20 Nov 2023.
33. Schöberl J. NETGEN an advancing front 2D/3D-mesh generator based on abstract rules. *Comput Vis Sci*. 1997;1(1):41–52.
34. Staehle S, Rebl H, Nebe B. Phenotypic stability of the human MG-63 osteoblastic cell line at different passages. *Cell Biol Int*. 2019;43(1):22–32.
35. Guarino VA, Oldham WM, Loscalzo J, Zhang Y-Y. Reaction rate of pyruvate and hydrogen peroxide: assessing antioxidant capacity of pyruvate under biological conditions. *Sci Rep*. 2019;9(1):19568.
36. Kapuscinski J. DAPI: a DNA-specific fluorescent probe. *Biotech Histochem*. 1995;70(5):220–33.
37. Chaudière J, Ferrari-Illiou R. Intracellular antioxidants: from chemical to biochemical mechanisms. *Food Chem Toxicol*. 1999;37(9–10):949–62.
38. Staehle S, Koertge A, Nebe B. Intracellular calcium dynamics dependent on defined microtopographical features of titanium. *Biomaterials*. 2015;46:48–57.
39. Bienert GP, Chaumont F. Aquaporin-facilitated transmembrane diffusion of hydrogen peroxide. *Biochim Biophys Acta*. 2014;1840(5):1596–604.
40. Budde K, Zimmermann J, Neuhaus E, Schroder M, Uhrmacher AM, van Rienen U. Requirements for documenting electrical cell stimulation experiments for replicability and numerical modeling. *Annu Int Conf IEEE Eng Med Biol Soc*. 2019;2019:1082–8.
41. Ercan B, Webster TJ. Greater osteoblast proliferation on anodized nanotubular titanium upon electrical stimulation. *Int J Nanomedicine*. 2008;3(4):477–85.
42. Wang Y, Cui H, Wu Z, Wu N, Wang Z, Chen X, et al. Modulation of Osteogenesis in MC3T3-E1 cells by different frequency electrical stimulation. *PLoS One*. 2016;11(5):e0154924.
43. Caliri AW, Tommasi S, Besaratinia A. Relationships among smoking, oxidative stress, inflammation, macromolecular damage, and cancer. *Mutat Res Rev Mutat Res*. 2021;787:108365.
44. Schieke SM, von Montfort C, Buchczyk DP, Timmer A, Grether-Beck S, Krutmann J, et al. Singlet oxygen-induced attenuation of growth factor signaling: possible role of ceramides. *Free Radic Res*. 2004;38(7):729–37.
45. Winterbourn CC, Hampton MB. Thiol chemistry and specificity in redox signaling. *Free Radic Biol Med*. 2008;45(5):549–61.
46. Sies H. Hydrogen peroxide as a central redox signaling molecule in physiological oxidative stress: oxidative eustress. *Redox Biol*. 2017;11:613–9.
47. Stone JR, Yang S. Hydrogen peroxide: a signaling messenger. *Antioxid Redox Signal*. 2006;8(3–4):243–70.
48. Stadtman ER, Levine RL. Free radical-mediated oxidation of free amino acids and amino acid residues in proteins. *Amino Acids*. 2003;25(3–4):207–18.
49. Halliwell B. Cell culture, oxidative stress, and antioxidants: avoiding pitfalls. *Biom J*. 2014;37(3):99–105.
50. Joshi R, Adhikari S, Patro BS, Chattopadhyay S, Mukherjee T. Free radical scavenging behavior of folic acid: evidence for possible antioxidant activity. *Free Radic Biol Med*. 2001;30(12):1390–9.
51. Rubio CP, Cerón JJ. Spectrophotometric assays for evaluation of reactive oxygen species (ROS) in serum: general concepts and applications in dogs and humans. *BMC Vet Res*. 2021;17(1):226.
52. Zannetti A, Benga G, Brunetti A, Napolitano F, Avallone L, Pelagalli A. Role of Aquaporins in the physiological functions of mesenchymal stem cells. *Cells*. 2020;9(12)
53. Cortizo MC, de Mele MFL, Cortizo AM. Metallic dental material biocompatibility in osteoblastlike cells: correlation with metal ion release. *Biol Trace Elem Res*. 2004;100(2):151–68.
54. Johnson A, Shiraishi T. Biocompatibility of precious metals for medical applications. In: Baltzer N, Copponnex T, editors. *Precious metals for biomedical applications*. Amsterdam: Elsevier; 2014. p. 37–55. (Woodhead Publishing series in biomaterials; number 77).
55. McHardy J, Robblee LS, Marston JM, Brummer SB. Electrical stimulation with Pt electrodes. IV. Factors influencing Pt dissolution in inorganic saline. *Biomaterials*. 1980;1(3):129–34.
56. Martins AP, Ciancetta A, de Almeida A, Marrone A, Re N, Soveral G, et al. Aquaporin inhibition by gold(III) compounds: new insights. *ChemMedChem*. 2013;8(7):1086–92.
57. Martins AP, Marrone A, Ciancetta A, Galán Cobo A, Echevarría M, Moura TF, et al. Targeting aquaporin function: potent inhibition of aquaglyceroporin-3 by a gold-based compound. *PLoS One*. 2012;7(5):e37435.
58. Wu Z, Li S, Liu J, Shi Y, Wang J, Chen D, et al. RNAi-mediated silencing of AQP1 expression inhibited the proliferation, invasion and tumorigenesis of osteosarcoma cells. *Cancer Biol Ther*. 2015;16(9):1332–40.
59. Ozkucur N, Monsees TK, Perike S, Do HQ, Funk RHW. Local calcium elevation and cell elongation initiate guided motility in electrically stimulated osteoblast-like cells. *PLoS One*. 2009;4(7):e6131.
60. Liu Z, Dong L, Wang L, Wang X, Cheng K, Luo Z, et al. Mediation of cellular osteogenic differentiation through daily stimulation time based on polypyrrole planar electrodes. *Sci Rep*. 2017;7(1):17926.
61. Staehle S, Rebl H, Finke B, Mueller P, Gruening M, Nebe JB. Enhanced calcium mobilization in osteoblasts on amino group containing plasma polymer nanolayer. *Cell Biosci*. 2018;8:22.
62. Gruening M, Neuber S, Nestler P, Lehnfeld J, Dubs M, Fricke K, et al. Enhancement of intracellular calcium ion mobilization by moderately but not highly positive material surface charges. *Front Bioeng Biotechnol*. 2020;8:1016.
63. Xu X, Liu S, Liu H, Ru K, Jia Y, Wu Z, et al. Piezo channels: awesome mechanosensitive structures in cellular Mechanotransduction and their role in bone. *Int J Mol Sci*. 2021;22(12)
64. Orrenius S, Zhivotovsky B, Nicotera P. Regulation of cell death: the calcium-apoptosis link. *Nat Rev Mol Cell Biol*. 2003;4(7):552–65.
65. Zhivotovsky B, Orrenius S. Calcium and cell death mechanisms: a perspective from the cell death community. *Cell Calcium*. 2011;50(3):211–21.
66. Love MR, Palee S, Chattipakorn SC, Chattipakorn N. Effects of electrical stimulation on cell proliferation and apoptosis. *J Cell Physiol*. 2018;233(3):1860–76.
67. Gordeeva AV, Zvyagilskaya RA, Labas YA. Cross-talk between reactive oxygen species and calcium in living cells. *Biochemistry*. 2003;68(10):1077–80.
68. Görlach A, Bertram K, Hudecova S, Krizanova O. Calcium and ROS: a mutual interplay. *Redox Biol*. 2015;6:260–71.
69. Schalenbach M, Durmus YE, Tempel H, Kungl H, Eichel R-A. The role of the double layer for the pseudocapacitance of the hydrogen adsorption on platinum. *Sci Rep*. 2022;12(1):3375.
70. Doering M, Kieninger J, Kübler J, Hofmann UG, Rupitsch SJ, Urban GA, et al. Advanced electrochemical potential monitoring for improved understanding of electrical neurostimulation protocols. *J Neural Eng*. 2023;20(3):36036.

Publisher's Note

Springer Nature remains neutral with regard to jurisdictional claims in published maps and institutional affiliations.